



Published in final edited form as:

Science. 2019 October 25; 366(6464): 454–460. doi:10.1126/science.aax7526.

Spatiotemporal expansion of primary progenitor zones in the developing human cerebellum

Parthiv Haldipur¹, Kimberly A. Aldinger¹, Silvia Bernardo², Mei Deng³, Andrew E. Timms¹, Lynne M. Overman⁴, Conrad Winter¹, Steven N. Lisgo⁴, Ferechte Razavi⁵, Evelina Silvestri⁶, Lucia Manganaro², Homa Adle-Biasette⁷, Fabien Guilmiot⁸, Rosa Russo⁹, Debora Kidron¹⁰, Patrick R. Hof¹¹, Dianne Gerrelli¹², Susan J. Lindsay⁴, William B. Dobyns^{1,3}, Ian A. Glass^{1,3}, Paula Alexandre¹², Kathleen J. Millen^{1,3,*}

¹Center for Integrative Brain Research, Seattle Children's Research Institute, Seattle, USA.

²Departments of Experimental Medicine, and Radiological Sciences, Sapienza University of Rome, Rome, Italy.

³Department of Pediatrics, University of Washington, Seattle, USA.

⁴Institute of Genetic Medicine, Newcastle University, Newcastle upon Tyne, UK

⁵Hôpital Necker-Enfants Malades, APHP, Paris, France

⁶Surgical Pathology Unit, San Camillo Forlanini Hospital, Rome, Italy

⁷Department of Pathology, Hôpital Lariboisière, APHP, Paris, France

⁸Hôpital Robert-Debré, INSERM UMR 1141, Paris, France.

⁹Department of Pathology, University Medical Hospital, Salerno, Italy

¹⁰Department of Pathology, Meir Medical Center, Kfar Saba and Sackler School of Medicine, Tel Aviv University, Israel

¹¹Nash Family Department of Neuroscience and Friedman Brain Institute, Icahn School of Medicine at Mount Sinai, New York, USA

¹²University College London Great Ormond Street Institute of Child Health, UK.

Abstract

*Correspondence to: Kathleen J. Millen: kathleen.millen@seattlechildrens.org.

Author contributions: **Conceptualization:** PH, KJM; **Methodology:** PH, KAA, PA, KJM; **Software:** KAA, AET, PA; **Validation:** PH, LMO; **Formal analysis:** PH, PA, KAA, KJM; **Investigation:** PH, MD, CW, LMO, PA; **Resources:** SB, SNL, IAG, DG, SJL, DK, LM, RR, HAB, FR, ES; **Data Curation:** PH, KAA, AET; **Writing – original draft preparation:** PH, PA, KAA, KJM; **Writing – review and editing:** PH, KAA, PRH, PA, KJM; **Visualization:** PH, KAA, PA, WBD, KJM; **Supervision:** PH, KJM; **Project administration:** PH, KJM; **Funding acquisition:** KJM.

Data and materials availability: Human material provided by the Joint MRC/Wellcome (MR/R006237/1) Human Developmental Biology Resource (www.hdb.org), and the Birth Defects Research Laboratory (NIH-R24-HD000836 to IAG) was covered by a material transfer agreement between SCRI and HDBR/BDRL but samples may be requested directly from the HDBR/BDRL. Macaque images were provided by MacBrainResource: macbrainresource.org (NIMH-R01-MH113257 to AD and LS). Sequence data is available upon request and data deposited into dbGaP is under accession number phs001901.v1.p1.

Competing interests: Authors declare no competing interests.

We present histological and molecular analyses of the developing human cerebellum from 30 post-conception days to 9 postnatal months. Differences in developmental patterns between human and mouse include spatiotemporal expansion of both ventricular and rhombic lip primary progenitor zones to include sub-ventricular zones containing basal progenitors. The human rhombic lip persists longer through cerebellar development than in the mouse and undergoes morphological changes to form a progenitor pool in the posterior lobule, not seen in other organisms including the non-human primate, the macaque. Disruptions in human rhombic lip development are associated with posterior cerebellar vermis hypoplasia and Dandy-Walker malformation. The presence of these species-specific neural progenitor populations refine our insight into human cerebellar developmental disorders.

One Sentence Summary

A close look at human cerebellar development reveals species-specific neuronal progenitors that inform cerebellar disease pathogenesis.

Human cerebellar birth defects are common and often cause motor and cognitive disabilities, yet most knowledge of cerebellar development is from mice. The mouse cerebellum shares many features of lamination, circuitry, neuronal morphology and foliation with humans. However, the human cerebellum which contains 80% of all brain neurons, has 750-fold greater surface area, increased neuronal numbers, altered neuronal subtype ratios and increased folial complexity (1-3).

Human cerebellar development begins by 30 post-conception days and is complete by the end of the second postnatal year (4, 5). Mouse cerebellar development is nearly complete by postnatal day (P)15, following just 19 gestational days. While human development is protracted, this alone is unlikely to explain species differences. Cerebral cortical neurogenesis differs between these species, with humans having large numbers of outer radial glia in an outer-subventricular zone which drive human cortical expansion and gyrification (6, 7). Since neuronal numbers in the cerebellum and cerebral cortex scale across evolution (8), we expected divergent cerebellar neurogenesis programs across species.

Studies of human cerebellar development began prior to publication of photographic plates (9). Limited histological data is available from 10 post-conception weeks (pcw) through late gestation (4, 5, 10-12). Developmental neuroimaging atlases have been compiled from *in utero* MRI studies from gestational weeks (gw) 20-24 (18-22pcw) but are of limited resolution (13). Major gaps in available human data correspond to essential cerebellar developmental epochs defined in model vertebrates. Here we analyze human cerebellar development from post-conception day 30 to 9 postnatal months (Fig. 1; Table S1), define the timing of developmental events, and provide insight into cellular and molecular programs driving human cerebellar development.

Spatiotemporal expansion of human cerebellar progenitor zones

We surveyed morphology from human and mouse cerebellar sagittal vermis sections. Humans and mice both have two primary zones of neurogenesis: the ventricular zone (VZ)

and the rhombic lip (RL) (Figs. 1; S1A). The VZ gives rise to all GABAergic populations, including Purkinje cells. The RL gives rise to all cerebellar glutamatergic neurons. Cerebellar nuclei neurons are generated first, followed by granule cell progenitors of the external granule layer which proliferate, differentiate, and migrate to become granule neurons of the internal granule layer. Unipolar brush cells arise last (14). The human cerebellar anlage between Carnegie Stage (CS) 12 and CS23 (30- 56 days), resembles the mouse cerebellar anlage in size and shape, from embryonic day (E) 10.5-17.5 (Figs. 1; S1A). However, the mouse VZ thins between E10.5 and E15.5 (Fig. S1B-G) and the RL disappears by birth (E19/P0) (Fig. S1A). The human embryonic RL is small but the human VZ thickens through 10pcw. After 10 pcw, the VZ thins and the RL expands into an elongated tail-like structure. Between 11-13pcw, the elongated RL thickens, continuing to trail from the growing posterior vermis. Between 13-14pcw, the RL incorporates into the posterior lobule where it forms a densely packed pool of cells evident as late as 36pcw (Fig. 1).

The mouse external granule layer is evident by E12.5, with granule cell progenitor proliferation driving postnatal cerebellar and foliation expansion (15, 16). We detect initial external granule layer formation in the human cerebellum at 8 pcw (Fig. 2G, **EGL**) with primary and secondary fissure initiation apparent at 11 and 13pcw, respectively. Between 17pcw and birth (~36pcw) there is a ~5 fold increase in human cerebellar volume and folial complexity (17, 18). Peak proliferation in the human external granule layer occurs during the period between 26-32pcw (10).

Human cerebellum has a SVZ with basal progenitors

At CS12, the human cerebellar VZ resembles the E12.5 mouse VZ which displays a single zone of SOX2⁺, KI67⁺ progenitor cells spanning most of the anlage (Fig. 2A; S1B,F). By CS14, an emerging SVZ is evident (Fig. 2B). By CS18 and CS19, differentiating (TUJ1⁺, CTIP1⁺) neurons increase cerebellar anlage size (Fig. 2H,I). Increased differentiation in the outer SVZ diminishes SVZ size between CS21 and CS23 (Fig. 2E,F). By the end of embryogenesis, at 8pcw, only a residual VZ remains (Fig. 2G).

The expanded proliferative zone in the embryonic human cerebellum resembles the SVZ in the developing mouse and human cerebral cortex (19). The mouse cerebellar VZ does not have a SVZ. Instead, ventricular radial glial progenitors extend processes across the nascent anlage from the ventricular (apical) to the pial (basal) surface and undergo mitosis only at the ventricle (Fig. 2M-N; S1L-Q). In the human cerebellum, mitotic Phospho-histone H3⁺ progenitors are found within the VZ and SVZ, indicating the presence of basal progenitors which we have termed cerebellar basal progenitors (Fig. 2J-K, **red arrowhead; 2M**). Progenitors in both zones exhibit long radial processes which span the anlage thickness (Fig. 2N) and express mitotic radial glial marker phospho-vimentin (Fig. 2K). We see a significant expansion of cerebellar basal progenitors throughout the SVZ between CS18-23 (Fig. 2M), a time point coinciding with increased differentiation suggesting they could function as additional neurogenic progenitors.

Human cerebellar rhombic lip is long-lived and compartmentalized

Species differences in progenitor zone development are not restricted to the cerebellar VZ. We also identified differences in RL morphology, finding sub-structure in humans, including a split into ventricular (RL^{VZ}) and subventricular zones (RL^{SVZ}), and internalization (Fig. 3; S3A-G). The mouse RL is a proliferative, transient, dorsal stem cell zone, present between E12.5-E17.5, and composed entirely of KI67⁺ and SOX2⁺ stem cells lacking morphological compartmentalization (Fig. S2A-E). Although it is 5-8 cell layers thick, progenitor mitosis (PH3⁺ and phospho-Vimentin⁺) is confined to the single layer of cells lining the ventricle (Fig. S2G-L). In contrast, the human RL and its remnants are seen throughout gestation and display a more complex proliferation profile (Fig. S3A-G; S5C).

The human RL excludes VZ derived GABAergic neurons, expresses classic RL markers and is proliferative even when embedded within the posterior-most lobule of the cerebellum (Figs. 3A-H; 4B; S3A-K). The human embryonic RL, similar to the mouse, consists of KI67⁺ and SOX2⁺ cells (Figs. 4B-C, **CS18**; S2A-F). However, after 10pcw the human RL splits into a SOX2⁺ and KI67-rich RL^{VZ} (Fig. 4B,C; **red asterisk**) and a KI67-rich, SOX2-sparse RL^{SVZ} (Fig. 4B,C; **yellow asterisk**). The two RL progenitor zones are separated by a vasculature bed, discernable by 11pcw (Fig. S5A, B, **arrows**). Cells in the RL^{SVZ} apparently migrate into the external granule layer (Fig. 4B-C; S3H-I, **white arrowhead**).

Radial glial mitosis in the early human RL is confined to cells lining the ventricle (Fig. 4D-E; **CS18**), much like the mouse (Fig. S2G-L). However, following the split of the RL, mitotic progenitors with radial glia-like morphology (PH3⁺, phospho-vimentin⁺) are detected in both the RL^{VZ} and RL^{SVZ} (Fig. 4D-E, **13 pcw**). DiI and lentiviral labeling reveal diverse morphologies of RL basal progenitors including uni-, bi- and multipolar cells with radially and tangentially oriented processes (Fig. 4A,F).

Although the mouse RL lacks structural compartmentalization, it is molecularly compartmentalized. An interior Wntless (WLS⁺) and LMX1A⁺ compartment is continuous with the VZ and an exterior compartment links to the external granule layer (ATOHI⁺). A gradient of PAX6⁺ expression exists across the mouse RL with strongest expression in the exterior compartment. The core of the mouse RL is composed of proliferating LMX1A⁺ progenitors destined to become posterior vermis granule cell progenitors and unipolar brush cells. Early specified and differentiating unipolar brush cells in the core also express TBR2 (20, 21).

In humans, WLS expression is also largely restricted to RL^{VZ} cells, although scattered expression was seen in RL^{SVZ} cells (Figs. 3E; S4A-C). *LMX1A* is expressed throughout the embryonic RL (Fig. S4D), in both the RL^{VZ} and RL^{SVZ} at later stages (Figs. 3G; S4E-F). *LMX1A* is also expressed in RL-derived cerebellar nuclear and unipolar brush cell populations streaming into the cerebellar core as well as the choroid plexus epithelium (Fig. S4E). A sharp boundary between *LMX1A*, and *ATOHI* in RL exiting granule cell progenitors define the anterior limit of the RL (Figs. 3G-H; S4D-J). The posterior limit of the human RL is defined by *LMX1A*⁺, *MKI67*⁻ choroid plexus cells (Fig. S4D, G-H). PAX6 expression is predominant in the RL^{VZ}, although there is also extensive expression in the

RL^{SVZ}, with upregulation in nascent external granule layer cells streaming from the RL^{SVZ} (Figs. 3D; S4K-M). TBR2 is expressed throughout the RL^{SVZ} with a few scattered, presumably nascent unipolar brush cells, in both the external and internal granule layer (Figs. 3F; S4N-P).

Human RL progenitors share some similarities to mice

To provide an unbiased analysis of the molecular programs encoded by human RL progenitors, we profiled the human RL transcriptome using bulk sequencing from laser-capture microdissected RL^{VZ} and RL^{SVZ} (Data S1-S4). Principal component analysis (PCA) indicated age as the first principal component explaining 56% of the variance (Fig. 5A). Differential expression analysis between RL^{VZ} and RL^{SVZ} identified alterations in 622 genes (\log_2 fold change > 1.5 and Benjamini-Hochberg adjusted $P < 0.05$). The 374 genes upregulated in RL^{VZ} included *CRYAB*, *SOX2* and *WLS*, while the 248 genes upregulated in the RL^{SVZ} included *EOMES* (Fig. 5B; Data S2). We evaluated pathway enrichment of the upregulated genes and found RL^{VZ} genes were enriched in HIPPO and WNT signaling (Fig. 5C; Data S3). RL^{SVZ} genes were enriched in axon guidance and synaptic vesicle cycling (Data S4). Several known mouse marker genes for RL and early RL-derivates showed similar expression profiles in our samples (22) (Fig. S3L). We next compared genes with significant differential expression between the RL^{VZ} and RL^{SVZ} to mouse gene sets identified in the RL and RL-related cells in recent single cell analyses of the developing mouse cerebellum (23, 24). While roof plate-like stem cell genes and a subset of mouse RL genes were differentially expressed in the RL^{VZ}, genes expressed in mouse RL-, unipolar brush cell- and granule cell-progenitors were seen throughout the RL. Unipolar brush cell genes were highly expressed in the RL^{SVZ} indicating it likely is a reservoir for nascent human unipolar brush cells, in addition to other glutamatergic lineages (Figs. 5D-G; S3M). Our analyses validate our hypothesis that the spatiotemporally expanded structure in the posterior vermis is indeed the RL, and similarities in gene expression patterns exist between the mouse and human RL notwithstanding differences in structure.

RL spatiotemporal expansion may be a human-specific

The developing human and non-human primate cerebral cortex share an expanded SVZ relative to mice (25, 26). Since the brain weight to neuron number ratio does not differ significantly among primates, we expected non-human primates to share elaborated cerebellar progenitor zones (27, 28). We analyzed mid-sagittal sections of the developing cerebella of rhesus macaque (*Macaca mulatta*; 164 days gestation). The macaque RL at E48 resembles the embryonic CS23 RL in humans (Fig. S6A, S6M). However, as foliation initiates, the macaque RL regresses in a manner similar to the mouse RL and unlike humans (Fig. S6B,C). By mid- and late-gestation (E78-133), there is no evidence of RL expansion or morphological compartmentation (Fig. S6D-L). This suggests spatiotemporal expansion of the RL may be specific to human.

The internalized RL generates the posterior vermis

Human cerebellar volume increases 5-fold between 22pcw and birth, and it becomes highly foliated during the third trimester (24-40gw) (17, 18). Granule cell progenitor proliferation peaks during this period, accompanied by increased external granule layer thickness (5, 10). In mice, cerebellar growth and foliation are driven by granule cell progenitor proliferation between P1-14, with deficient proliferation causing external granule layer thinning, and reduced foliation and cerebellar volume (15, 16). Disproportionate reduction in posterior vermis volume is a feature of many human cerebellar birth defects, including Dandy-Walker malformation and cerebellar vermis hypoplasia (29). Mouse models have indicated that RL disruption in the form of precocious differentiation or aberrant migration of progenitors is central to posterior vermis hypoplasia (30-32). In mice and humans, ten cardinal lobules are grouped together into anterior, central and posterior lobes of the vermis defined by the primary and secondary fissure. In humans, all ten lobules are first identifiable between 14 and 18pcw. Development progresses from anterior to posterior, with the increase in posterior vermis size and folial complexity relative to the anterior cerebellum beginning only after 17pcw (Fig. 6A). The RL and its vestiges are detectable in human cerebella until birth. The longevity of the internalized RL thus correlates with growth and foliation of the human posterior vermis, a cerebellar region associated with human cognition (33).

To determine if RL abnormalities specifically contribute to posterior vermis hypoplasia in Dandy-Walker malformation and cerebellar vermis hypoplasia, we assessed 16 archival samples aged 17-30pcw (Table S1). All show delay or failure of posterior vermis growth. Most show only a partially formed posterior-most lobule (31). Although overall decreased external granule layer proliferation may contribute to this phenotype, peak external granule layer proliferation only begins around 26pcw (26-32pcw) and hypoplasia of the posterior vermis is evident earlier (Figs. 6B-H; S7A-P) (30, 31, 34). Indeed, Dandy-Walker malformation and cerebellar vermis hypoplasia are routinely diagnosed *in utero* around 17pcw (35). The RL is absent in half of our cases and delayed (not internalized) or reduced in size and cellularity in the others (Fig. 6H). Among cerebella lacking a RL, ~62% are older than 21pcw, when the human RL is normally still present. We conclude that while the early RL (<13pcw) contributes granule cell progenitors to the external granule layer which later proliferate to drive expansion of the anterior cerebellum, the older, internalized RL (>14pcw) generates granule cell progenitors required to fully elaborate the posterior vermis during mid and late gestation.

Preterm brain injury is associated with cerebellar abnormalities (36, 37). We find RL^{VZ} and RL^{SVZ} are separated by a vascular bed beginning at 11pcw, when the RL itself is elongated and perhaps more vulnerable to insult. Vascular insults causing RL structural damage from 13-14pcw onwards likely contribute to these neurodevelopmental abnormalities. Thus, although mouse studies were essential to spotlight a role for the RL in human Dandy-Walker malformation, the underlying pathological mechanisms can likely never be fully modeled in mice which lack complex RL anatomy. Similarly, our discovery of previously undescribed progenitor populations and the longevity of the RL in the human cerebellum suggests mouse models of the cells of origin for some groups of medulloblastoma, a cerebellar tumor, may also be inadequate (38). Our studies underline the urgency of further comparative cellular

and molecular analyses of human and mouse cerebellar development to define better the value and limitations of mouse genetic models of human neurodevelopmental disorders.

Supplementary Material

Refer to Web version on PubMed Central for supplementary material.

ACKNOWLEDGEMENTS

We thank Berta Lopez, Nadia Moreno, Moira Crosier, Yuzhu Cheng, Jacqui Dobor (HDBR), Diana O'Day (UW), Alexandria Sjoboen, Jake Millman, Derek Dang, Danilo Dubocanin (SCRI) Bridget Wicinski (Hof laboratory), Dr Adrian Thrasher (UCL), Drs. Alvaro Duque and Lynn Selemom (MacBrainResource) and NIHR GOSH Biomedical Research Centre for providing resources and technical help. We are grateful to Prof David Price (Edinburgh) for recommending HDBR, and Prof Shubha Tole (TIFR, India) for her feedback on the manuscript.

Funding: This work was supported by NIH-R01-NS080390 and R01-NS095733 to KJM and R01-N5050375 to WBD. PH was awarded EMBO fellowship:ATSF-431-2016, Burroughs-Wellcome Fund:1018771, Company of Biologists Fellowship:DEVTF190393 and National Ataxia Foundation Young Investigator Research Grant. PA was awarded the Newlife Charity for disabled children Start-Up Grant:SG/17-18/05.

References

1. Lange W, Cell number and cell density in the cerebellar cortex of man and some other mammals. *Cell Tissue Res* 157, 115 (1975). [PubMed: 804353]
2. Van Essen DC, Surface-based atlases of cerebellar cortex in the human, macaque, and mouse. *Ann N Y Acad Sci* 978, 468 (12, 2002). [PubMed: 12582074]
3. Larsell O. a. J. J., *The Comparative Anatomy and Histology of the Cerebellum The Human Cerebellum, Cerebellar Connections and Cerebellar Cortex*. University of Minnesota Press Minneapolis, (1972).
4. Haldipur P et al., Preterm delivery disrupts the developmental program of the cerebellum. *PLoS One* 6, e23449 (2011). [PubMed: 21858122]
5. Rakic P, Sidman RL, Histogenesis of cortical layers in human cerebellum, particularly the lamina dissecans. *J Comp Neurol* 139, 473 (8, 1970). [PubMed: 4195699]
6. Molnar Z, Pollen A, How unique is the human neocortex? *Development* 141, 11 (1, 2014). [PubMed: 24346696]
7. Nowakowski TJ, Pollen AA, Sandoval-Espinosa C, Kriegstein AR, Transformation of the Radial Glia Scaffold Demarcates Two Stages of Human Cerebral Cortex Development. *Neuron* 91, 1219 (9 21, 2016). [PubMed: 27657449]
8. Herculano-Houzel S, Coordinated scaling of cortical and cerebellar numbers of neurons. *Front Neuroanat* 4, 12 (2010). [PubMed: 20300467]
9. Larsell O, Stotler WA, Some morphological features of the human cerebellum. *Anat Rec* 97, 352 (3, 1947).
10. Abraham H, Tornoczky T, Kosztolanyi G, Seress L, Cell formation in the cortical layers of the developing human cerebellum. *Int J Dev Neurosci* 19, 53 (2, 2001). [PubMed: 11226755]
11. Haldipur P et al., Expression of Sonic hedgehog during cell proliferation in the human cerebellum. *Stem Cells Dev* 21, 1059 (5 1, 2012). [PubMed: 21732818]
12. Zecevic N, Rakic P, Differentiation of Purkinje cells and their relationship to other components of developing cerebellar cortex in man. *J Comp Neurol* 167, 27 (5 01, 1976). [PubMed: 818132]
13. Habas PA et al., A spatiotemporal atlas of MR intensity, tissue probability and shape of the fetal brain with application to segmentation. *Neuroimage* 53, 460 (11 1, 2010). [PubMed: 20600970]
14. Leto K et al., Consensus Paper: Cerebellar Development. *Cerebellum* 15, 789 (12, 2016). [PubMed: 26439486]

15. Corrales JD, Rocco GL, Blaess S, Guo Q, Joyner AL, Spatial pattern of sonic hedgehog signaling through Gli genes during cerebellum development. *Development* 131, 5581 (11, 2004). [PubMed: 15496441]
16. Dahmane N, Ruiz i Altaba A, Sonic hedgehog regulates the growth and patterning of the cerebellum. *Development* 126, 3089 (6, 1999). [PubMed: 10375501]
17. Limperopoulos C et al., Late gestation cerebellar growth is rapid and impeded by premature birth. *Pediatrics* 115, 688 (3, 2005). [PubMed: 15741373]
18. Volpe JJ, Cerebellum of the premature infant: rapidly developing, vulnerable, clinically important. *J Child Neurol* 24, 1085 (9, 2009). [PubMed: 19745085]
19. Pollen AA et al., Molecular identity of human outer radial glia during cortical development. *Cell* 163, 55 (9 24, 2015). [PubMed: 26406371]
20. Chizhikov VV et al., Lmx1a regulates fates and location of cells originating from the cerebellar rhombic lip and telencephalic cortical hem. *Proc Natl Acad Sci U S A* 107, 10725 (6 8, 2010). [PubMed: 20498066]
21. Yeung J et al., Wls provides a new compartmental view of the rhombic lip in mouse cerebellar development. *J Neurosci* 34, 12527 (9 10, 2014). [PubMed: 25209290]
22. Morales D, Hatten ME, Molecular markers of neuronal progenitors in the embryonic cerebellar anlage. *J Neurosci* 26, 12226 (11 22, 2006). [PubMed: 17122047]
23. Vladoiu MC et al., Childhood cerebellar tumours mirror conserved fetal transcriptional programs. *Nature* 572, 67 (8, 2019). [PubMed: 31043743]
24. Wizeman JW, Guo Q, Wilton EM, Li JY, Specification of diverse cell types during early neurogenesis of the mouse cerebellum. *Elife* 8, (2 8, 2019).
25. Florio M, Huttner WB, Neural progenitors, neurogenesis and the evolution of the neocortex. *Development* 141, 2182 (6, 2014). [PubMed: 24866113]
26. Lui JH, Hansen DV, Kriegstein AR, Development and evolution of the human neocortex. *Cell* 146, 18 (7 8, 2011). [PubMed: 21729779]
27. Azevedo FA et al., Equal numbers of neuronal and nonneuronal cells make the human brain an isometrically scaled-up primate brain. *J Comp Neurol* 513, 532 (4 10, 2009). [PubMed: 19226510]
- 28.erculano-Houzel S, The human brain in numbers: a linearly scaled-up primate brain. *Front Hum Neurosci* 3, 31 (2009). [PubMed: 19915731]
29. Barkovich AJ, Millen KJ, Dobyns WB, A developmental and genetic classification for midbrain-hindbrain malformations. *Brain* 132, 3199 (12, 2009). [PubMed: 19933510]
30. Aldinger KA et al., FOXC1 is required for normal cerebellar development and is a major contributor to chromosome 6p25.3 Dandy-Walker malformation. *Nat Genet* 41, 1037 (9, 2009). [PubMed: 19668217]
31. Haldipur P et al., Phenotypic outcomes in Mouse and Human Foxc1 dependent Dandy-Walker cerebellar malformation suggest shared mechanisms. *Elife* 6, (1 16, 2017).
32. Haldipur P et al., Foxc1 dependent mesenchymal signalling drives embryonic cerebellar growth. *Elife* 3, (12 16, 2014).
33. Schmahmann JD, Guell X, Stoodley CJ, Halko MA, The Theory and Neuroscience of Cerebellar Cognition. *Annu Rev Neurosci* 42, 337 (7 8, 2019). [PubMed: 30939101]
34. Bernardo S et al., Dandy-Walker Malformation: is the 'tail sign' the key sign? *Prenat Diagn* 35, 1358 (12, 2015). [PubMed: 26448595]
35. Poretti A, Boltshauser E, Huisman T, Pre- and Postnatal Neuroimaging of Congenital Cerebellar Abnormalities. *Cerebellum* 15, 5 (2, 2016). [PubMed: 26166429]
36. Aldinger KA et al., Redefining the Etiologic Landscape of Cerebellar Malformations. *Am J Hum Genet*, (8 28, 2019).
37. Pichiecchio A et al., "Acquired" Dandy-Walker malformation and cerebellar hemorrhage: Usefulness of serial MRI. *Eur J Paediatr Neurol* 20, 188 (1, 2016). [PubMed: 26507178]
38. Azzarelli R, Simons BD, Philpott A, The developmental origin of brain tumours: a cellular and molecular framework. *Development* 145, (5 14, 2018).

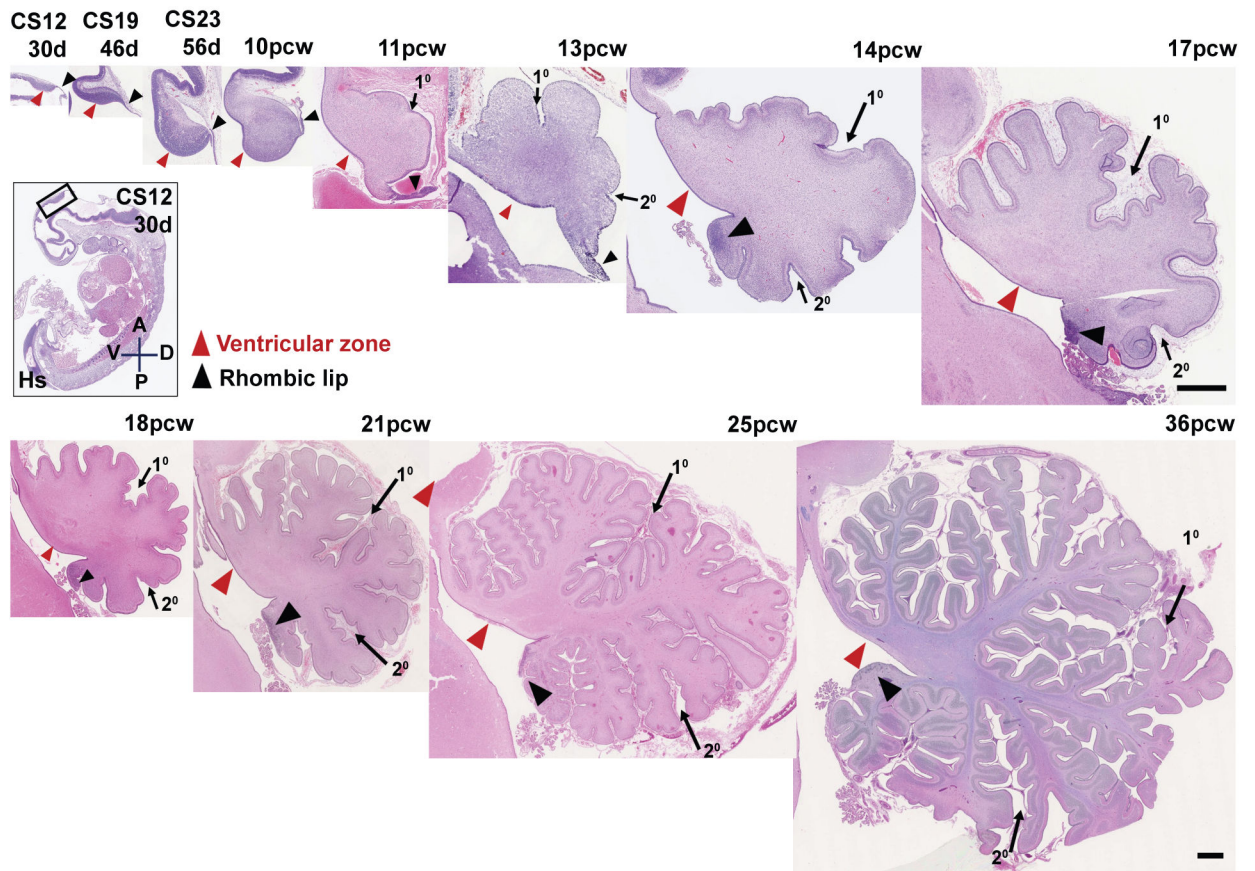


Fig. 1: An outline of human cerebellar development.

H&E-stained midsagittal sections of the developing human cerebellum. The two main zones of neurogenesis, the ventricular zone (red arrowhead) and rhombic lip (black arrow head) are marked. Primary and secondary fissures are noted (arrows). Scale bar = 100 μ m

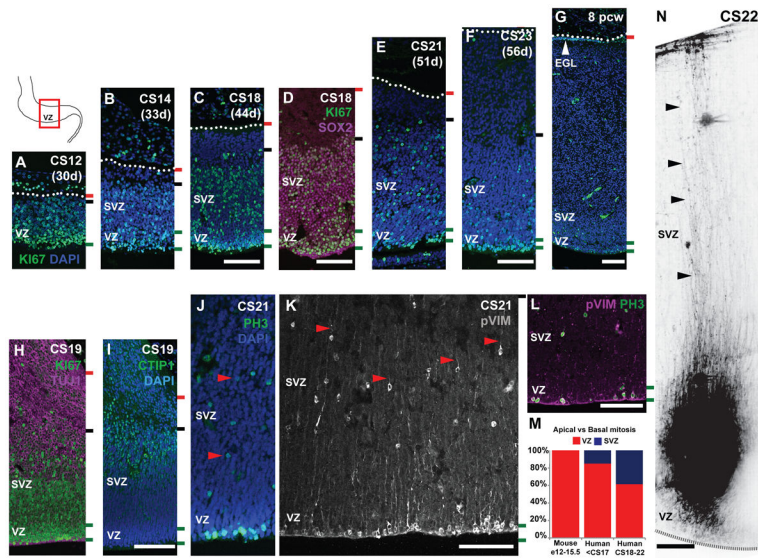


Fig. 2: The human cerebellar VZ is expanded into a SVZ.

Midsagittal sections of the human embryonic cerebellum stained with KI67 (A-G) and SOX2 (D), reveal VZ expansion. (H) β -III Tubulin (TUJ1) and CTIP1 (I) expression suggest neuronal differentiation beginning around CS19 takes place in the SVZ. (G) External granule layer (EGL) first appears at 8pcw. (J-L) Mitosis and mitotic radial glia are observed in both the VZ and SVZ as evidenced by phospho-histone H3 (PH3) (J) and phospho-vimentin (pVIM) (K, L) expression. (M) A significant increase in the proportion of cerebellar basal progenitors (J-K, red arrowheads) is seen between the human and mouse cerebellum, and between CS18-23 (Chi-square, df: 132.5, 2; P value <0.0001). (N) DiO labeling of VZ/SVZ progenitors at CS22 show radial glial fibers traversing the thickness of the cerebellum. Sections were counterstained using DAPI. Green and black dashed lines and the dotted line mark the boundaries of the VZ, SVZ and pia respectively. Scale bar = 100 μ m.

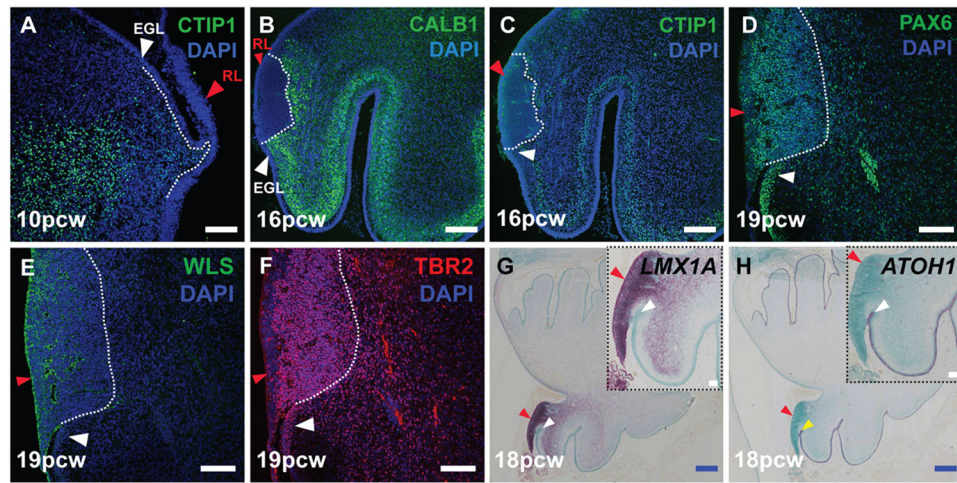


Fig. 3: The human cerebellar rhombic lip expresses classic markers.

(A) VZ born Purkinje cells expressing CTIP1 (A,C) and Calbindin (B) migrate around the RL (red arrowhead). The RL expresses classic markers like PAX6 (D), WLS (E), TBR2 (F) and *LMX1A* (G). (H) *ATOH1* is expressed by cells exiting the RL into the external granule layer (white arrowhead). Sections were counterstained with DAPI (A-F) and Fast green (G,H). Scale bar = 100 μm (white), 500 μm (blue).

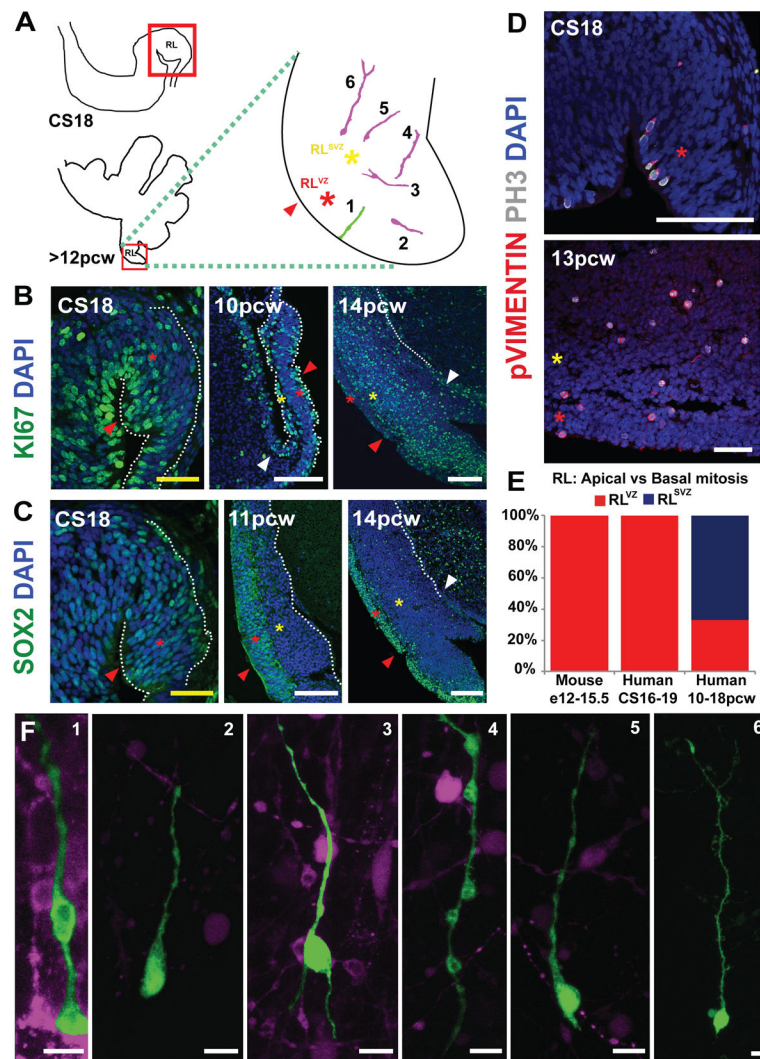


Fig. 4: The human cerebellar RL is compartmentalized into ventricular and subventricular zones.

(A) Illustration of the cerebellar regions studied in this figure. The RL (red arrowhead) is expanded into ventricular (RL^{VZ}, red asterisk) and subventricular zones (RL^{SVZ}, yellow asterisk). (B) KI67 expression reveals extensive proliferation in the RL. (C) The RL is compartmentalized into a SOX2-rich RL^{VZ} and SOX2-sparse RL^{SVZ}. (D) Phosphohistone-H3 and phospho-vimentin expression indicate the presence of mitotic ventricular and subventricular-basal progenitors. (E) The proportion of basal progenitors increases significantly following the splitting of the RL (Chi-square, df: 137.8, 2; P value <0.0001). (F) DiI and lentiviral labeling of an organotypic slice of the human cerebellum reveal diverse morphologies of RL ventricular and basal progenitors. Scale bar = 100 μ m (white), 50 μ m (yellow).

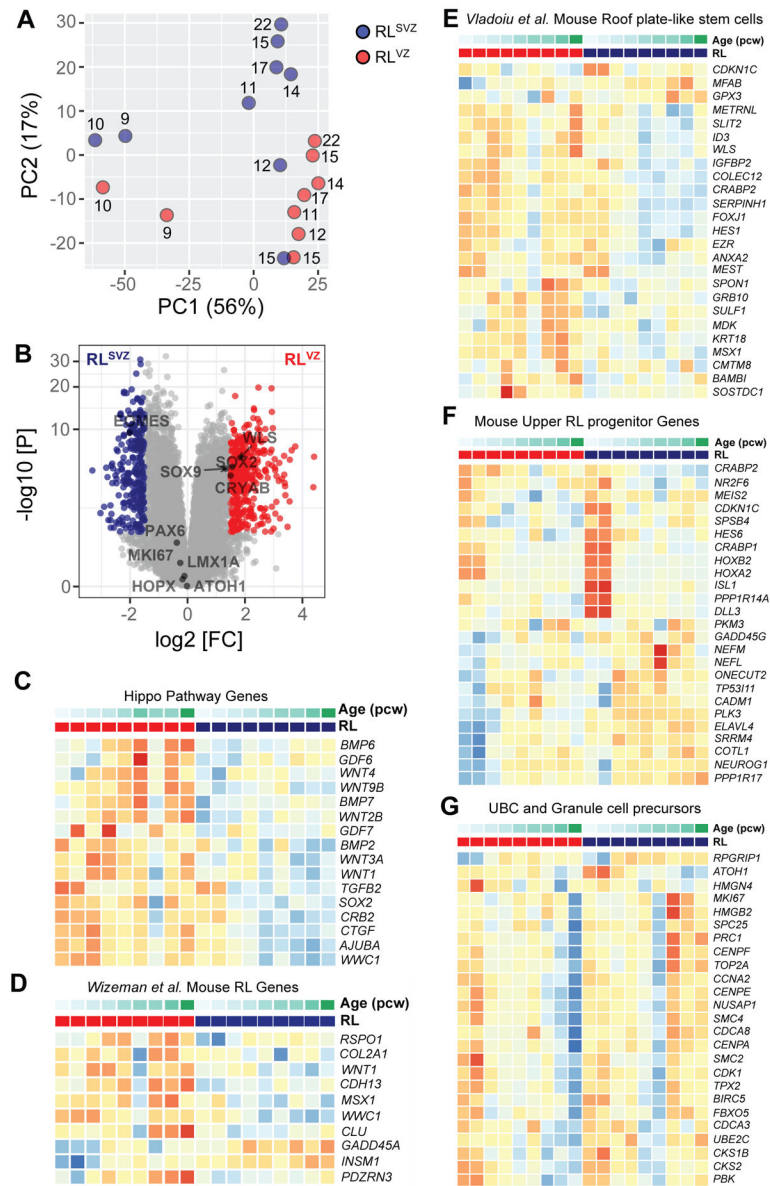


Fig. 5: RNA-seq of human RL compartments.

(A) Principal component (PC) analysis indicates the largest source of variation among the RNA-seq samples was age accounting for 56% of the variance in the data. Samples microdissected from RL^{SVZ} are blue and RL^{VZ} are red. The numbers beside each circle represent sample age (pcw). (B) Volcano plot illustrating differential expression of genes in RL^{VZ} versus RL^{SVZ}. Red and blue dots represent genes expressed significantly higher in RL^{VZ} or RL^{SVZ}, respectively. (C-G) Heatmaps of gene expression for each human sample. Samples are grouped by RL^{VZ} (red) and RL^{SVZ} (blue), then ascending age (9-22pcw). (C) Expression of Hippo pathway genes and (D-G) top genes for RL-related cell clusters identified by single-cell RNA-sequencing of the mouse cerebellum from E10-P14 (23,24).

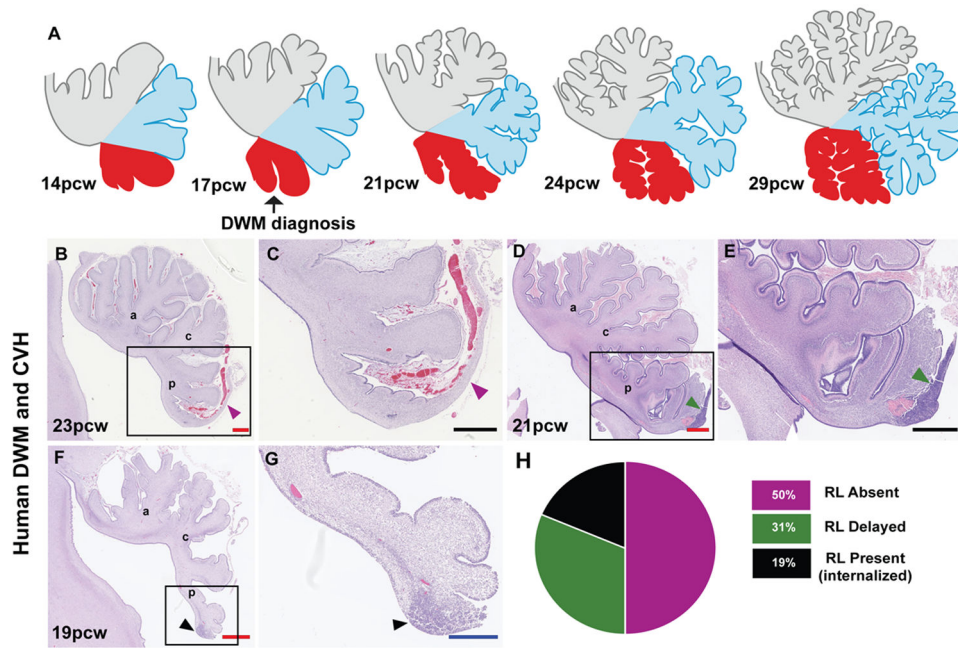


Fig. 6: Internalized RL may be a feature specific to human cerebellar development.

(A) Model for human cerebellar development indicates growth of the posterior vermis correlates with spatiotemporal RL expansion. (B-G) Analysis of H&E-stained sagittal sections of the human cerebellum from cases diagnosed with Dandy-Walker malformation (DWM) and cerebellar vermis hypoplasia (CVH) indicates the RL is absent in 50% of cases (B,C) while being severely diminished remaining cases (D-G). The anterior (a), central (c) and posterior lobes (p) are indicated. (H) Pie chart representing the absence of RL in 50% of tested samples. Scale bar = 100 μ m (black), 0.5 mm (blue) and 1 mm (red).